ADVANCED INTELLIGENT SYSTEMS
Open Access
www.advintellsyst.com

Independent Control and Path Planning of Microswimmers with a Uniform Magnetic Field

*Lucas Amoudruz and Petros Koumoutsakos**

Artificial bacteria flagella (ABFs) are magnetic helical microswimmers that can be remotely controlled via a uniform, rotating magnetic field. Previous studies have used the heterogeneous response of microswimmers to external magnetic fields for achieving independent control. Herein, analytical and reinforcement learning control strategies for path planning to a target by multiple swimmers using a uniform magnetic field are introduced. The comparison of the two algorithms shows the superiority of reinforcement learning in achieving minimal travel time to a target. The results demonstrate, for the first time, the effective independent navigation of realistic microswimmers with a uniform magnetic field in a viscous flow field.

1. Introduction

The magnetic control of microswimming devices[1–5] through micromanipulation,[6,7] targeted drug delivery,[8,9] or convection-enhanced transport,[10] has created new frontiers for biomedicine. A particularly promising technology involves corkscrew-shaped magnetic microswimmers (artificial bacterial flagella (ABFs)) that propel themselves when subjected to a rotating magnetic field.[11] Rotating magnetic fields can form propulsive gradients and they are arguably preferable to alternatives, such as electric fields, for in vivo conditions.[12,13] However, the independent, yet coordinated, control of individual ABFs is challenging as it requires balancing between the magnetic forces and the hydrodynamic interactions between the swimmers while the employed magnetic fields are practically uniform over lengths of few micrometers. We note that independent navigation of mm-sized microswimmers has been shown in ref. [14] through experiments and simulations, while in ref. [15], a reinforcement learning (RL) algorithm was applied to adjust the velocity of an idealized swimmer in simulations with one way coupling with a complex flow field. Control of swimmers using two-way coupling and RL have been demonstrated with linked-spheres at low Reynolds numbers[16] and for artificial fish in macroscales.[17] Similarly, genetic algorithms have been used to navigate microswimmers toward high concentrations of chemicals.[18]

The problem of heterogeneous microrobots navigation via a uniform input has been studied in two dimensions on surfaces[19] and in a fluid at rest.[20] The steering of two micropropellers along two distinct paths in three dimensions has been accomplished with the help of magnetic fields gradients.[21] These advances exploited the heterogeneous response of microswimmers to a uniform input to achieve independent trajectories along a prescribed path. These control methods are based on short horizon objectives (stay on the prescribed path) and do not provide the trajectory that minimizes the travel time to a target position, particularly in the presence of a background flow. In addition, strong background flows restrict the set of feasible paths for given micro-swimmers. To the best of our knowledge the steering of multiple micron-sized swimmers towards a target in a minimal time under a background flow and a uniform magnetic field has not been reported before.

In this work, we present two methods to independently guide two micro-ABFs towards a single target in the presence of a uniform magnetic field. The two methods rely on simulations of swimming ABFs using an ordinary differential equation (ODE) model. The model is calibrated with the method of dissipative particle dynamics (DPD),[22,23] taking into account the particular geometry of the swimmers and their interactions with the viscous fluid. We first present a semi-analytical solution for the simple yet instructive setup of multiple, geometrically distinct ABFs in free space, with zero background flow. This result enables understanding of the design constraints for the ABFs necessary for independent control and how their geometric characteristics relate to their travel time. We then employ RL to control multiple ABFs trajectories in a broad range of flow conditions including a nonzero background flow.

2. Artificial Bacterial Flagella

The ABFs are modeled as microscopic rigid bodies of length l with position $\mathbf{x}$ and orientation q (represented by a quaternion), immersed in a viscous fluid and subjected to a rotating, uniform, magnetic

L. Amoudruz, P. Koumoutsakos
Computational Science and Engineering Laboratory
ETH Zürich
Zurich CH-8092, Switzerland
E-mail: petros@seas.harvard.edu

L. Amoudruz, P. Koumoutsakos
John A. Paulson School of Engineering and Applied Sciences
Harvard University
Cambridge MA 02134, MA, USA

The ORCID identification number(s) for the author(s) of this article can be found under https://doi.org/10.1002/aisy.202100183.

DOI: 10.1002/aisy.202100183

field. We estimate that the magnetic and hydrodynamic interactions between ABFs are orders of magnitude smaller than those due to the magnetic field for dilute systems (see Supporting Information) and we ignore inertial effects due to their low Reynolds number ($\mathrm{Re} \approx 10^{-3}$). Following this approximation, the system is fully described by the position and orientation of the ABFs.

Additionally, the linear and angular velocities of the ABF, $\mathbf{V}^b$ and $\mathbf{\Omega}^b$, are directly linked to the external force and torque, $\mathbf{F}^b$ and $\mathbf{T}^b$, via the mobility matrix[24]

$$\begin{bmatrix} \mathbf{V}^b \\ \mathbf{\Omega}^b \end{bmatrix} = \begin{bmatrix} \Delta & Z \\ Z^{\mathrm{T}} & \Gamma \end{bmatrix} \begin{bmatrix} \mathbf{F}^b \\ \mathbf{T}^b \end{bmatrix} \tag{1}$$

where the superscript $\boldsymbol{b}$ indicates that the quantity is expressed in the ABF frame of reference, for which Δ, Z, and Γ are diagonal. The matrices Γ and Z represent the application of torque to changing the angular and linear velocity, respectively. The ABFs are propelled by torque applied through a magnetic field and we assume that it can swim only in the direction of its main axis so that Z has only one nonzero entry (Z_{11}). The coefficients in the mobility matrix are often estimated by empirical formulas for low Reynolds number flows.[25] Here we estimate the components of the mobility matrix for the specific ABF by conducting flow simulations using DPD,[22,23] which we validate against experimental data of ref. [8] (see Supporting Information). We remark that the shape (pitch, diameter, length, thickness) of the ABF influence the elements of these matrices and the present approach allows to account for these geometries.

The ABF with a magnetic moment $\mathbf{m}$ is subjected to a uniform magnetic field $\mathbf{B}$ and hence experiences a torque

$$\mathbf{T} = \mathbf{m} \times \mathbf{B} \tag{2}$$

No other external force is applied to the ABF, hence $\mathbf{F} = \mathbf{0}$. Combining Equation (1) with the kinematic equations for a rigid body gives the following system of ODEs

$$\dot{\mathbf{x}} = \mathbf{V} \tag{3a}$$

$$\dot{q} = \frac{1}{2} q \otimes \hat{\mathbf{\Omega}} \tag{3b}$$

$$\mathbf{V}^b = Z\mathbf{T}^b \tag{3c}$$

$$\mathbf{\Omega}^b = \Gamma\mathbf{T}^b \tag{3d}$$

where $\otimes$ denotes the quaternion product, and $\hat{\mathbf{\Omega}}$ the pure quaternion formed by the vector $\mathbf{\Omega}$. The transformations between the laboratory frame of reference and that of the ABF are given by

$$\mathbf{T}^b = R(q)\mathbf{T} \tag{4a}$$

$$\mathbf{m} = R(q^\star)\mathbf{m}^b \tag{4b}$$

$$\mathbf{V} = R(q^\star)\mathbf{V}^b \tag{4c}$$

$$\mathbf{\Omega} = R(q^\star)\mathbf{\Omega}^b \tag{4d}$$

where $q^\star$ is the conjugate of q and $R(q)$ is the rotation matrix that corresponds to the rotation by a quaternion q.[26] The system of differential Equation (2) and (3) is advanced in time with a fourth order Runge–Kutta integrator.

We note that when simulating multiple noninteracting ABFs in free space, we use the above ODE system for each swimmer with the common magnetic field but different mobility coefficients and magnetic moments.

3. Forward Velocity

ABFs were designed to swim under a rotating, uniform magnetic field.[11,27] We first study this scenario by applying the field $\mathbf{B}(t) = B(0, \cos\omega t, \sin\omega t)$ to ABFs initially aligned with the x axis of the laboratory frame. Note that in the later sections, the magnetic field is able to rotate in any direction so that the swimmers can navigate in three dimensions. We consider two ABFs with the same length but different pitch and magnetic moments, as shown in **Figure 1**. In both cases, the magnetic moment is perpendicular to the helical axis of the ABF. Under these conditions, by symmetry of the problem, the swimmers swim along the x axis. The difference in pitch results in different coefficients of the mobility matrix and along with the different magnetic moments results in distinct propulsion velocities for the two ABFs. For each ABF velocity, we distinguish a linear and a non-linear variation with respect to the frequency of the magnetic field. First, the ABF rotates at the same frequency as the magnetic field and its forward velocity increases linearly with the frequency of the magnetic field, consistent with the low Reynolds approximation.[3,8,28,29] In the nonlinear regime, the magnetic torque is no longer able to sustain the same frequency of rotation as the magnetic field. The onset of nonlinearity

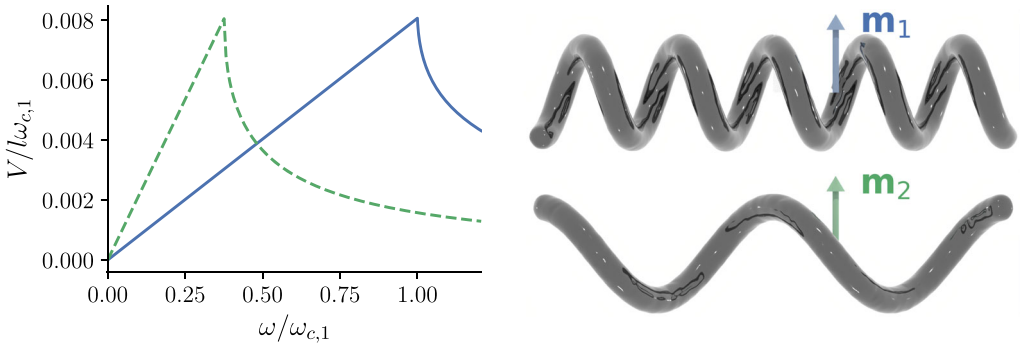

Figure 1. Left: Dimensionless time averaged forward velocity of two ABFs, differing in shape and magnetic moment, against the field rotation frequency (in units of the step-out frequency of the first swimmer, $\omega_{c,1}$). Right: The ABFs geometries. The arrows represent the magnetic moment of the ABFs.

depends on the geometry and magnetic moment of the ABF as well as the imposed magnetic field. Indeed, the magnitude of the magnetic torque is bounded while that of the hydrodynamic torque increases linearly with the ABF angular velocity Ω. The torque imbalance at high rotation frequencies causes the ABF to slip, resulting in an alternating forward and backward motion (see Supporting Information). Increasing the frequency further increases the effective slip and accordingly decreases the forward velocity. The two regimes are distinguished by the step-out frequency ω_c corresponding to the maximum forward velocity of the ABF.

The differences in propulsion velocities for the ABFs can be exploited to control independently their trajectories. The slope V/ω in the linear regime depends only on the shape of the ABF. The step-out frequency depends on both the shape and the magnetic moment (it can also be changed by varying the surface wetability of the ABF[30]). These two properties can be chosen such that the forward velocities of two ABFs react differently to the magnetic rotation frequency (Figure 1). By changing ω, it is then possible to control the relative velocities of the two ABFs: one is faster that the other in one regime while the opposite occurs in an other regime. This simple observation constitutes the key idea for independent control of several ABFs even with a uniform magnetic field. We remark that, while this potential has been previously identified,[28,30–33] the control of similar systems have been performed in the simple case of free space, non interacting propellers and no background flow.[20,21] To the best of our knowledge, this is the first time that such independent controlled navigation of multiple microswimmers is materialised in three dimensions with a complex background flow. In the following sections we propose two methods to tackle the problem of steering ABFs toward a target in a minimal amount of time.

4. Independent Control I: Semianalytical Solution

In the absence of an external flow field, we derive a semianalytical strategy for the navigation of N ABFs toward a particular target. Each ABF has a distinct magnetic moment and without any loss of generality, we set the target position of all swimmers to the origin and define the initial position of the ith ABF as $\mathbf{x}^{(i)}$. We assume that the time required by one ABF to align with the rotation direction of the field is much smaller than $|\mathbf{x}^{(i)}|/v$, where v is the typical forward velocity of the ABF. The proposed strategy consists in gathering all ABFs along one direction $\mathbf{n}_k$ at a time, such that $\mathbf{x}^{(i)} \cdot \mathbf{n}_k = 0,\ i = 1, 2, \ldots, N$ after phase k. We choose a sequence of orthogonal directions, $\mathbf{n}_k \cdot \mathbf{n}_{k'} = \delta_{kk'}$. The choice of the orientations of $\mathbf{n}_k$ is not restricted to the basis vectors of the laboratory frame and is described at the end of this section. In three dimensions, the strategy consists of three phases, $k = 1, 2, 3$, until all ABFs have reached their target: they first gather on a plane, then on a line and finally to the target.

All ABFs are gathered along a given direction $\mathbf{n}_k$ by exploiting the different forward responses of the ABFs when we alternate the frequency of rotation of the magnetic field. More specifically, for N ABFs, the field rotates in the direction $\mathbf{n}_k$ for t_j time units at frequency $\omega_{c,j},\ j = 1, 2, \ldots, N$, where $\omega_{c,j}$ is the step-out frequency of the jth swimmer. We define the velocity matrix with elements $U_{ij} = V_i(\omega_{c,j})$, denoting the velocity of swimmer i when the field rotates with the step out frequency of swimmer j. We can relate the above quantities to the (signed) distances d_j covered by the ABFs as

$$d_i = \sum_{j=1}^{N} s_j t_j U_{ij} \tag{5}$$

where $s_j \in \{-1, 1\}$ determines if the field rotates clockwise/counterclockwise. Equivalently, the vector form of the above is $\mathbf{d} = U\boldsymbol{\beta}$, where $\beta_j = t_j s_j$. Setting $d_i = \mathbf{x}^{(i)} \cdot \mathbf{n}_k$, we can invert this linear system of equations for each phase k and obtain the times spent at each step-out frequency $\boldsymbol{\beta} = U^{-1} X \mathbf{n}_k$, where we have set $X_{ij} = x_j^{(i)}$. We emphasize that this result holds only if the velocity matrix is invertible, restricting the design of the ABFs to achieve independent control. The total time spent at phase k is then given by

$$T(\mathbf{n}_k) = \sum_{i=1}^{N} t_i = \sum_{i=1}^{N} |\beta_i| = \| U^{-1} X \mathbf{n}_k \|_1 \tag{6}$$

The yet unknown directions $\mathbf{n}_k$, $k = 1, 2, 3$, are chosen to minimize the total travel time. The directions are parameterized as $\mathbf{n}_k = R(\phi, \theta, \psi)\mathbf{e}_k,\ k = 1, 2, 3$, where $R(\phi, \theta, \psi)$ is the rotation matrix given by the three Euler angles ϕ, θ and ψ. Note that this choice of handedness of the three directions does not influence the final result. The optimal angles satisfy

$$\phi^\star, \theta^\star, \psi^\star = \mathrm{argmin}_{\phi,\theta,\psi} \sum_{k=1}^{3} T(R(\phi, \theta, \psi)\mathbf{e}_k) \tag{7}$$

We solve the above minimization problem numerically with derandomised evolution strategy with covariance matrix adaptation (CMA-ES)[34] (see Supporting Information for the configuration of the optimizer).

5. Independent Control II: Reinforcement Learning

We now employ a RL approach to solve the problem introduced in section 4. Each of the N ABFs is initially placed at a random position $\mathbf{x}_i \sim \mathcal{N}(\mathbf{x}_i^0, \sigma),\ i = 1, 2, \ldots, N$. The RL agent controls the magnetic field frequency of rotation and direction, and has the goal of bringing all ABFs within a small distance (here two body lengths, $d = 2l$) from the target origin. This small distance is justified by the assumption of noninteracting ABFs. The agent sets the direction and magnitude of the magnetic field frequency every fixed time interval. An episode is terminated if either of the two conditions occur: a) all ABFs reached the target within a small distance d, or b) the simulation time exceeds a maximum time $T_{\max}$. The positions $\mathbf{x}_i$ and orientations q_i of the ABFs describe the state s of the environment in the RL framework. The action performed by the agent every Δt time encodes the magnetic field rotation frequency and orientation for the next time interval. The

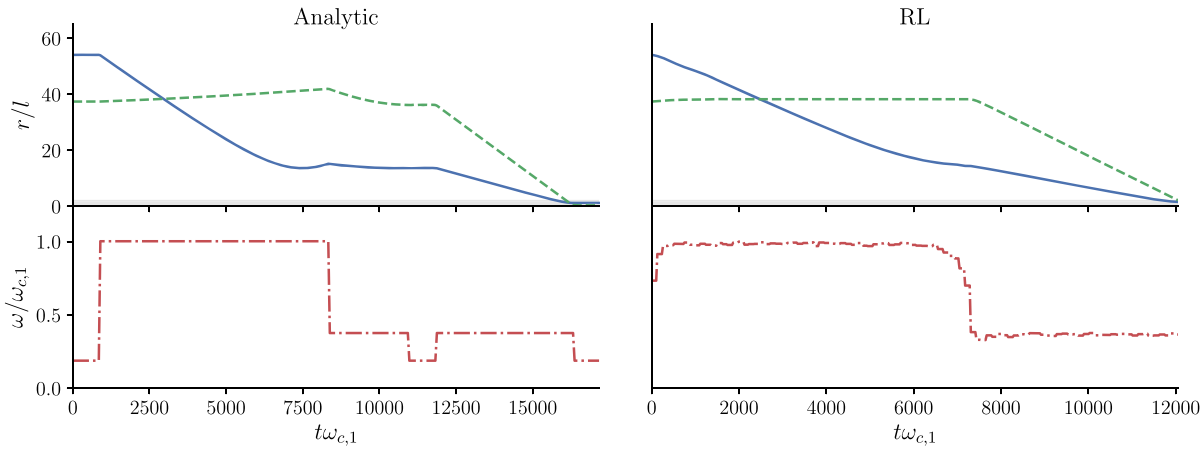

Figure 2. Distance to target of the two controlled ABFs (in units of body length l) against dimensionless time (——— and - - - -) in free space, zero background flow, and corresponding magnetic field rotation frequency (— · —), where $\omega_{c,1}$ is the step-out frequency of the first swimmer.

reward of the system is designed so that all ABFs reach the target and the travel time is minimized. Additionally, a shaping reward term[35] is added to improve the learning process. The training is performed using VRACER, the off-policy actor critic RL method described in ref. [36] More details on the method can be found in the Supporting Information.

6. Reaching the Targets

In this section, we demonstrate the effectiveness of the two methods introduced in Sections 4 and 5. We first consider 2 ABFs in free space with zero background flow. **Figure 2** shows the distance of the ABFs to their target over time, and the corresponding magnetic field rotation frequency for both methods. In both cases, the ABFs successfully reach their target. Interestingly, the rotation frequencies chosen by the RL agent correspond to the step-out frequencies of the ABFs. Indeed, these frequencies allow the fastest absolute velocity difference between the ABFs, so it is consistent that they are part of the fastest solution found by the RL method. Furthermore, the RL trained swimmer was about 25% faster than the semianalytical swimmer. We remark that the RL solution amounts to first blocking the forward motion of one swimmer while the other continues swimming (see **Figure 3**). The blocked swimmer is first reoriented such that its magnetic moment is orthogonal to the plane of the magnetic field rotation, thus the resulting magnetic torque applied to this swimmer is zero. On the other hand, the method presented in Section 4 makes both ABFs swim at all time, even if one of them must go further from its target. In such situations, the "blocking" method found by RL is advantageous over the other method.

We now employ the RL method in the case of 2 ABFs swimming in a background flow with nonzero velocity. The assumptions required for deriving the semianalytical approach are violated and therefore we do not use this approach in this case.

In the presence of a background flow $\mathbf{u}_\infty$, Equation (4c) and (4d) become

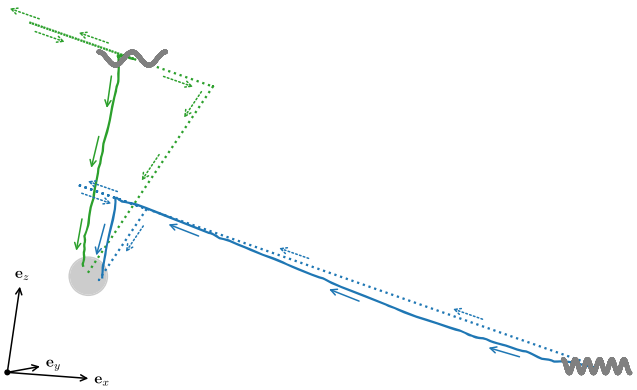

Figure 3. Trajectories of the ABFs from their initial positions (ABF representations) to the target area (sphere) obtained with the two methods in three dimensions : semianalytical (dotted lines) and RL (solid lines). The arrows show the successive axes of rotation of the magnetic field. The size of the ABFs has been scaled up by a factor of 7, for visualization purpose.

$$\begin{aligned}\mathbf{V} &= R(q^\star)\mathbf{V}^b + \mathbf{u}_\infty(\mathbf{x}) \\ \mathbf{\Omega} &= R(q^\star)\mathbf{\Omega}^b + \tfrac{1}{2}\nabla\times\mathbf{u}_\infty(\mathbf{x}) + \tfrac{\lambda^2-1}{\lambda^2+1}\mathbf{p}\times(E(\mathbf{x})\mathbf{p})\end{aligned} \tag{8}$$

where we approximated the rotation component by the effect of the flow on an axisymmetric ellipsoid of aspect ratio λ (Jeffery orbits). Here $E(\mathbf{x}) = (\nabla\mathbf{u}_\infty(\mathbf{x}) + \nabla\mathbf{u}_\infty^T(\mathbf{x}))/2$ is the deformation rate tensor of the background flow evaluated at the swimmer's position and $\mathbf{p} = R(q^\star)\mathbf{e}_x$ is the orientation of the ellipsoid. We used $\lambda = 2$ in the subsequent simulations. The background flow is set to the initial conditions of the Taylor-Green vortex

$$\mathbf{u}_\infty(\mathbf{r}) = \begin{bmatrix} A\cos ax \sin by \sin cz \\ B\sin ax \cos by \sin cz \\ C\sin ax \sin by \cos cz \end{bmatrix} \tag{9}$$

with $A = B = C/2 = V_1(\omega_{c,1})$ and $a = b = -c = 2\pi/50l$. With these parameters, the maximum velocity of the background flow is larger than the maximum swimming speed of the ABFs.

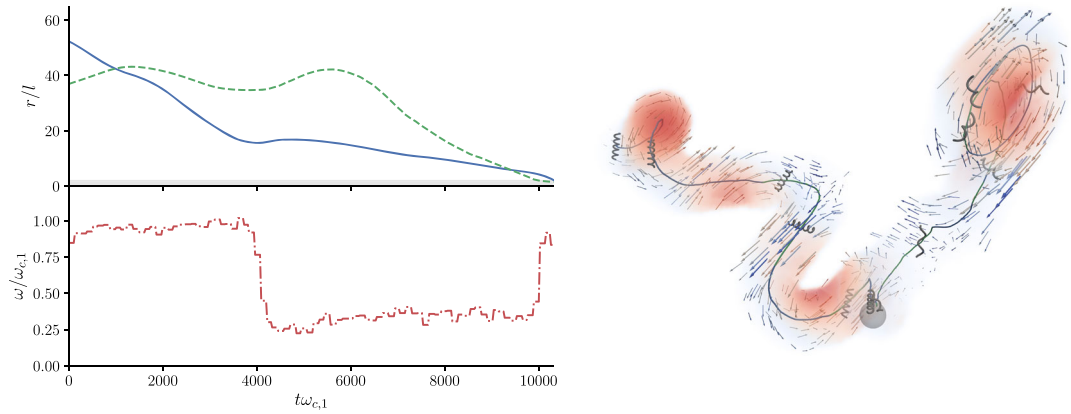

Figure 4. Left: Distance to target of the two controlled ABFs (in units of body length l) against dimensionless time (——— and - - - -) in free space with the background flow described by Equation (9) and corresponding magnetic field rotation frequency (— · —), where $\omega_{c,1}$ is the step-out frequency of the first swimmer. Right: Trajectories of the ABFs with nonzero flow obtained with the RL method. The arrows represent the velocity field and the colors represent the magnitude of the vorticity field. The flow field is only shown for a distance less than $4l$ from the trajectories, where l is the length of the swimmers.

The distances between the swimmers and the target over time are shown for the RL method on **Figure 4**. Despite the background flow perturbation, the RL method successfully navigates the ABFs to their target. The magnetic action space exhibits a similar behavior as in the free space case: the rotation frequency of the magnetic field oscillates between the step out frequencies of both swimmers and never exceeds the highest of these frequencies, where the swimming performance would degrade considerably. The trajectories of the ABFs seem to make use of the velocity field to achieve a lower travel time: Figure 4. shows that the trajectories tend to be parallel to the velocity field. The RL method not only found a solution, but also made use of its environment to reduce the travel time.

7. Robustness of the RL Policy

The robustness of the RL method is tested against two external perturbations, unseen during the training phase. In both cases, the robustness of the method is measured in terms of success rate (expected ratio between the number of successful trajectories and the number of attempts). First, a flow perturbation $\boldsymbol{\delta}\mathbf{u}(\mathbf{r}) = \varepsilon \mathbf{u}_\infty(\mathbf{r}/p)$ is added to the background flow described in the previous section, where ε controls the strength of the perturbation and p controls the wave length of the perturbation with respect to the original one. **Figure 5** shows the success rate of the RL approach against the perturbation strength ε for different p. For large wave lengths ($p = 2$), the RL agent is able to successfully steer the ABFs to their target in more than 90% of the cases when the perturbation strengths of less than 20% of the original flow. In contrast, the success rate degrades more sharply for smaller wave lengths ($p = 1/2$), suggesting that the method is less robust for short wave length perturbations. The RL policy seems more robust to perturbations with the same wavelengths as the original flow ($p = 1$) for large perturbation strengths: the success rate is above 30% even for large perturbations.

At small length scales, microswimmers are subjected to thermal fluctuations. We investigate the robustness of the RL policy (trained with the background flow, Equation (9)) on swimmers subjected to thermal noise and background flow (Equation (9)). The thermal fluctuations are modeled as an additive stochastic term to the linear and angular velocities of each

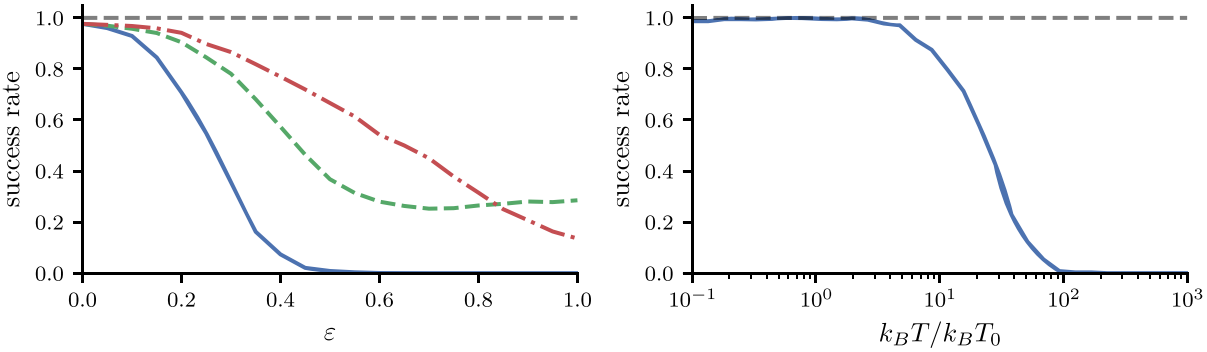

Figure 5. Left: Success rate of the RL method to guide swimmers to their target against the flow perturbation strength ε, for different wave numbers, $p = 1/2$ (———), $p = 1$ (- - - -), $p = 2$ (— · —). Right: Success rate of the RL method to steer swimmers to their target against thermal fluctuation $k_B T/k_B T_0$.

swimmer, following the Einstein relation with the mobility tensor given by Equation (1). Defining the generalized undisturbed velocity $\overline{\mathcal{V}} = (\mathbf{V}, \mathbf{\Omega})$, the resulting stochastic generalized velocities satisfy

$$\begin{aligned} &\mathcal{V} = \overline{\mathcal{V}} + \delta\mathcal{V}, \\ &\langle \delta\mathcal{V}_i \rangle = 0, \ i = 1, 2, \ldots, 6, \\ &\langle \delta\mathcal{V}_i, \delta\mathcal{V}_j \rangle = k_B T M_{ij}, \ i,j = 1, 2, \ldots, 6, \end{aligned} \tag{10}$$

where M is the mobility tensor and $k_B T$ is the temperature of the system, in energy units. The above property is achieved by adding a scaled Gaussian random noise with zero mean to the velocities at every time step of the simulation. The success rate of the policy is shown in Figure 5 for various temperatures $k_B T$, in units of the room temperature $k_B T_0$. As expected, a large thermal noise causes the policy to fail at its task. Nevertheless, this failure only occurs at relatively high temperatures: the success rate falls below 50% for $k_B T > 25 k_B T_0$, which is well above the normal operating conditions of ABFs. With temperatures below $2 k_B T_0$, the RL method sustains a success rate above 99%. We remark that this robustness is achieved successfully even with a policy trained with $k_B T = 0$.

8. Conclusion

We have presented two methods to guide multiple ABFs individually toward targets with a uniform magnetic field. The semi-analytical method allows to understand the basic mechanisms that allow independent control and we derive the necessary condition for the independent control of multiple ABFs: their velocity matrix must be invertible, a condition that can be accommodated by suitably choosing the geometries of the swimmers. This result may help to optimize the shapes of ABFs to further reduce the travel time.

The RL approach can control multiple ABFs in quiescent flow as well as in the presence of a complex background flow. Additionally, this approach is resilient to small flow perturbations and to thermal noise. When the background flow vanishes, the RL method recovers a very similar behavior as the first method: the rotation frequency is alternating between the step-out frequencies of the swimmers. Furthermore, the RL method could reach lower travel time than the first method by blocking one swimmer while the other is swimming. Steering an increased number of swimmers requires longer travel times according to the first method. We thus expect that applying the RL approach to more than two swimmers requires longer training times and might become prohibitively expensive as the number of swimmers increases. Possible solutions to this problem might include pre-training the RL agent with the policy found by the semi-analytical method.

The current work focused on the simplified case of non-interacting swimmers. In practice, the ABFs may interact hydrodynamically and magnetically with each other, encounter obstacles, evolve in confined geometries or experience time varying flows. Nevertheless, we expect the RL method to be a good candidate to overcome these variants, in the same way as it naturally handled the addition of a background flow.

Supporting Information

Supporting Information is available from the Wiley Online Library or from the author.

Acknowledgements

The authors acknowledge insightful discussions with Guido Novati (ETHZ) and his technical support for the usage of *smarties*. The authors acknowledge support by the European Research Council (ERC Advanced Grant 341117).

Conflict of Interest

The authors declare no conflict of interest.

Data Availability Statement

The data that support the findings of this study are openly available in msode at https://github.com/cselab/msode, with DOI number: 10.5281/zenodo.5801920.

Keywords

magnetically driven, microswimmers, reinforcement learning

Received: September 29, 2021
Revised: November 27, 2021
Published online:

[1] Q. Cao, X. Han, L. Li, *Lab Chip* **2014**, *14*, 2762.
[2] L. Yang, L. Zhang, *Annu. Rev. Control Rob. Auton. Syst.* **2021**, *4*, 1.
[3] P. Tierno, R. Golestanian, I. Pagonabarraga, F. Sagués, *J. Phys. Chem. B* **2008**, *112*, 16525.
[4] Y. Liu, D. Ge, J. Cong, H.-G. Piao, X. Huang, Y. Xu, G. Lu, L. Pan, M. Liu, *Small* **2018**, *14*, 1704546.
[5] P. Liao, L. Xing, S. Zhang, D. Sun, *Small* **2019**, *15*, 1901197.
[6] L. Zhang, K. E. Peyer, B. J. Nelson, *Lab Chip* **2010**, *10*, 2203.
[7] Y. Yu, J. Guo, Y. Wang, C. Shao, Y. Wang, Y. Zhao, *ACS Appl. Mater. Interfaces* **2020**, *12*, 16097.
[8] R. Mhanna, F. Qiu, L. Zhang, Y. Ding, K. Sugihara, M. Zenobi-Wong, B. J. Nelson, *Small* **2014**, *10*, 1953.
[9] P. Sharan, A. Nsamela, S. C. Lesher-Pérez, J. Simmchen, *Small* **2021**, *17*, 2007403.
[10] S. Schuerle, A. P. Soleimany, T. Yeh, G. M. Anand, M. Häberli, H. E. Fleming, N. Mirkhani, F. Qiu, S. Hauert, X. Wang, B. J. Nelson, S. N. Bhatia, *Sci. Adv.* **2019**, *5*, 4.
[11] L. Zhang, J. J. Abbott, L. Dong, B. E. Kratochvil, D. Bell, B. J. Nelson, *Appl. Phys. Lett.* **2009**, *94*, 064107.
[12] H. Gu, Q. Boehler, D. Ahmed, B. J. Nelson, *Sci. Rob.* **2019**, *4*, 35.
[13] K. Bente, A. Codutti, F. Bachmann, D. Faivre, *Small* **2018**, *14*, 1704374.
[14] D. Wong, E. B. Steager, V. Kumar, *IEEE Rob. Autom. Lett.* **2016**, *1*, 554.
[15] S. Colabrese, K. Gustavsson, A. Celani, L. Biferale, *Phys. Rev. Lett.* **2017**, *118*, 15.
[16] A. C. H. Tsang, P. W. Tong, S. Nallan, O. S. Pak, *Phys. Rev. Fluids* **2020**, *5* 074101.
[17] S. Verma, G. Novati, P. Koumoutsakos, *Proc. Natl. Acad. Sci.* **2018**, *115*, 5849.

[18] B. Hartl, M. Hübl, G. Kahl, A. Zöttl, *Proc. Natl. Acad. Sci.* **2021**, *118*, 19.
[19] S. Floyd, E. Diller, C. Pawashe, M. Sitti, *Int. J. Rob. Res.* **2011**, *30*, 1553.
[20] P. J. Vach, S. Klumpp, D. Faivre, *J. Phys. D: Appl. Phys.* **2015**, *49*, 065003.
[21] E. Diller, J. Giltinan, M. Sitti, *Int. J. Rob. Res.* **2013**, *32*, 614.
[22] P. Espanol, P. Warren, *EPL (Europhys. Lett.)* **1995**, *30*, 191.
[23] D. Alexeev, L. Amoudruz, S. Litvinov, P. Koumoutsakos, *Comput. Phys. Commun.* **2020**, 107298.
[24] J. Happel, H. Brenner, *Low Reynolds number hydrodynamics: With special applications to particulate media*, vol. *1*, Springer Science & Business Media, Berlin **1981**.
[25] S. Kim, S. J. Karrila, *Microhydrodynamics: Principles and selected applications*, Courier Corporation, Cambridge **2013**.
[26] B. Graf, arXiv preprint arXiv:0811.2889 **2008**.
[27] A. Ghosh, P. Fischer, *Nano Lett.* **2009**, *9*, 2243.
[28] K. E. Peyer, L. Zhang, B. J. Nelson, *Nanoscale* **2013**, *5*, 1259.
[29] D. Li, M. Jeong, E. Oren, T. Yu, T. Qiu, *Robotics* **2019**, *8*, 87.
[30] X. Wang, C. Hu, L. Schurz, C. De Marco, X. Chen, S. Pané, B. J. Nelson, *ACS Nano* **2018**, *12*, 6210.
[31] F. Bachmann, K. Bente, A. Codutti, D. Faivre, *Phys. Rev. Appl.* **2019**, *11*, 034039.
[32] I. S. Khalil, A. F. Tabak, Y. Hamed, M. E. Mitwally, M. Tawakol, A. Klingner, M. Sitti, *Adv. Sci.* **2018**, *5*, 1700461.
[33] I. S. Khalil, A. F. Tabak, Y. Hamed, M. Tawakol, A. Klingner, N. El Gohary, B. Mizaikoff, M. Sitti, *IEEE Rob. Autom. Lett.* **2018**, *3*, 1703.
[34] N. Hansen, S. D. Müller, P. Koumoutsakos, *Evol. Comput.* **2003**, *11*, 1.
[35] A. Y. Ng, D. Harada, S. Russell, in ICML, vol. *99*, **1999**, pp. 278–287.
[36] G. Novati, P. Koumoutsakos, in *Proceedings of the 36th Int. Conf. on Machine Learning*, Long Beach, CA, USA, 9–15 June **2019**.